Detailed Modeling of a Practical 1400MW Hydropower Plant and Real-Time Hardware Emulation For Governor Tuning Application

Ritu Tiwari, *Student Member, IEEE*, Thanga Raj Chelliah, *Senior Member, IEEE* and Venkata Dinavahi, *Fellow, IEEE*

***Abstract*—This paper presents the detailed nonlinear mathematical model of a 1400MW hydro power plant (HPP) and it's faster than real-time dynamic emulation on hardware architecture of the field programmable gate arrays (FPGA). This model is used to study the interactive effect of hydro turbine governor system (HTGS) and power system stabilizer (PSS) in nonlinear hydro-mechanical and electrical coupled (HMEC) system during low frequency oscillations. The Hopf bifurcation technique is employed for oscillation stability study and to obtain the optimum and stable operating region of the PID controller in the governor. Furthermore, oscillation damping is enhanced by improved tuning of PSS considering governor's servo motor time delay and frequency dead-band. The methodology for improved HTGS and PSS tuning provides 10 sec faster frequency stability with higher positive oscillation damping. Improved stability is illustrated using frequency deviation and generator active power results. The model accuracy is validated using 1400MW HPP field data. HMEC dynamic model of HPP is implemented on reconfigurable parallel hardware architecture of the FPGA board Xilinx® Virtex UltraScale+™, having the system solution pipelined for parallel computation, thus obtaining 49 times faster than real-time solution. This FPGA emulated prototype provides an advanced testing environment for new control strategies, system security assessment, predictive analyses of faults using real-time data, and plant optimization.**

***Index Terms*—Hydro power plant (HPP), hydro-mechanical and electrical coupled (HMEC), hydro turbine governing system (HTGS), field programmable gate arrays (FPGAs), Runge-Kutta 4th order (RK4), dynamic simulation, bifurcation theory, static excitation system (ST5B), power system stabilizer (PSS), Faster than real-time systems.**

I. Introduction

HYDROPOWER plants are very crucial source of electric supply, having near to zero carbon emissions and an abundant generation capacity for the future [1], [2]. The total installed capacity of HPPs in India is 46GW, which is about 11% of total electricity generation. With increasing renewable energy integration in the grid HPPs are envisioned to accommodate for upcoming challenges like generation reliability, peak demand control, primary frequency and inertial support for better dynamic stability and auxiliary support. In grid connected HPP during disturbances electro-mechanical and hydro-mechanical oscillations are most dominant; they become even more hazardous when resonate with each other [3]. Extensive study on several oscillation problem in HPP of different frequency ranges are reported in literature [4]– [8]. In [6], [9] the effect of nonlinearities like water elasticity, dead-band and servo motor delay during oscillatory and transient stability is studied.

In [5] effect of governor's gain in HPP and thermal plant frequency dead-band to inter-area oscillation damping is presented. However, no dead-band in hydro governors is assumed for the study which is not the case for most of the HPPs. In [6] effect of servomotor actuator uncertainties on very low frequency oscillation instability during black-start is observed and damping of oscillation is attained using robust governor PI tuning. In [7] for a particular length of penstock, water-conduit modes and penstock vibrations frequency overlaps with electromechanical modes and resonance is observer. In [8], [10] vortex rope pulsation (during part load) resonance with electromechanical modes specifically intra and local modes is discussed. In [9] water elasticity effects on oscillation damping capability of PSS is presented. In [10] nonlinear HTGS and penstock model is used for governor's PID tuning for load-rejection stability in a SMIB system.

It is observed from these literatures that various oscillatory instability and its resonance with other modes of oscillations are highly dependent on the HMEC system design parameters, control and system components nonlinearities, and system operating point. However, most of these studies used linearised models for a particular modal oscillation analysis while neglecting several nonlinearities to reduce complexity and computation burden. Such linearised and simplified models might fail for other case of oscillatory or transient instability analysis. Table.1 presents the detailed comparison of various HPP models in literature.

From the referred literature, it is concluded multi-machine model with HMEC system including an elastic model of penstock (for water hammer effect), nonlinear model of turbine, nonlinear governor and the higher order model of synchronous machine with detailed excitation system and PSS to have a nonlinear HPP model closer to the real system is still lacking.

This work is supported by the Natural Science and Engineering Research Council of Canada (NSERC), Hydropower Simulation Laboratory (HSL) of Indian Institute of Technology Roorkee, and THDC India Limited, Rishikesh, India.

R. Tiwari is a visiting Ph.D. student in the Department of Electrical and Computer Engineering, University of Alberta, Edmonton, Alberta from Indian Institute of Technology Roorkee (IITR), India.
T.R. Chelliah is with the Department of Water Resource Development and Management, Indian Institute of Technology Roorkee (IITR), Roorkee, India.
V. Dinavahi is with the Department of Electrical and Computer Engineering, University of Alberta, Edmonton, Alberta, Canada. Email: rtiwari1@ualberta.ca, thangfwt@iitr.ac.in, dinavahi@ualberta.ca.

TABLE I
COMPARISON OF HPP MODELS IN VARIOUS LITERATURE

Ref.	Generator model order	AVR order	PSS	Governor	Turbine	Penstock (elastic)	Stability study	Validation	
								FMV	RTI
3	1st	×	×	LM	NLM	✓	VRO and EM	×	×
5	1st ROLM	1st	PSS4B	LM	×	×	Inter-area	×	×
6	2nd SSM	1st	Washout filter only	NLM	LM	×	VLF during black start	×	×
7	1st ROLM	1st	Washout filter only	LM	LM	✓	WC and EMO	FMV	×
8	5th order	HOM	PSS2B	×	LM	✓	VRO and EMO	FMV	×
9	3rd ROLM	HOM	HOM	LM	LM	✓	×	×	×
10	1st	×	×	NLM	NLM	×	HTGS PID	×	×
Proposed model (NDE)	6th order	ST5B	PSS3B	NLM	NLM	✓	LFO	FMV	FTRT

∗ ROLM - Reduced order linear model ∗ HOM- Higher order model ∗ LM- Linear model ∗ NLM- Non-linear model ∗ FMV - Field measurement verification ∗ SSM- State space model ∗ VLF- Very low frequency ∗ WC- Water conduit ∗ VRO- Vortex rope oscillation ∗ LFO – Low frequency oscillation ∗ FTRT - Faster than real-time.

Also, there is need for an accurate HPPs model that can be used for reliable real-time implementation to better investigate the coupling patterns and factors of various hydro-mechanical with electro-mechanical oscillations [11]. Although most of the HPP components are included however, two assumptions of no surge tank and separate water way system for each turbine are considered in the proposed model. These assumptions can affect very-low frequency oscillation stability analysis for high-head (above 200m) and long penstock water conduit systems. Therefore, in this paper detailed multi machine nonlinear HMEC model of HPP is proposed to analyse the effect of nonlinear parameters of HMEC on transient and oscillation stabilities; moreover use this model for control parameters tuning for better stability. The accuracy of proposed model is validated with field measurements from 1400MW HPP. This paper also bridges the research gap of HMEC HPP multi-machine model, faster than real-time emulation on FPGA board that can be used as a laboratory prototype for different oscillation stability study,state estimation between real-time measurements and hardware-in-the-loop implementation.

A. System under study and problem description

In this paper as shown in Fig.1 1400MW Tehri Koteshwar HPP is used for study. HPP comprises of 8 synchronous generators, 4 at Tehri station rated 250MW each and the other 4 are at Kotehswar rated 100MW each, connected to grid by 400kV, 178km long double circuit transmission lines (TLs). The detailed mathematical model is presented in section II. Field data measurements collected during a 3-phase fault that lead to inter-area oscillation of around 0.6Hz reported in NRLDC report [12] is used for model validation. These oscillation also lead to 400MW peak to peak power oscillation at the plant level causing disturbance in guide vane opening, mechanical power and subsequently lead to the shutdown of 250MW generator at Tehri HPP. To damp inter-area oscillation tuning of ST5B [13] and PSS3B [13] for better transient stability are studied in [14], but without considering the nonlinear HTGS and HMEC system that considerably affect the plant stability during transients. This paper therefore uses the HMEC system to tune PID of the governor for better stability while also retuning PSS for better enhanced oscillation damping to compensate for the governor's time delay.

B. Control strategy and real-time hardware emulation

As the HTGS is represented using higher dimensional nonlinear differential equations the study of PID parameters stability region becomes extremely tedious due to tremendous computational demand by conventional methods, such as the center manifold method, normal form theory, and Lyapunov-Schmidt (L-S) method. In nonlinear complex system the robust analysis of stability in case of sustained oscillations due to variation in operation condition or parameters can be effectively studied using Hopf bifurcation [15], [16]. The stability study of HTGS using Hopf bifurcation is also gaining interest due to ease of computation, efficient elimination of oscillations, and flexibility with the size of the system [18], [19]. The HPP model under study is a 7-dimensional nonlinear system with time delay; the Hopf bifurcation technique with a known time delay system is proposed to predict the bifurcation points of the PID controller in the governor and the bifurcation curve is used for tuning the PID controller. The tuned and validated HPP model is implemented in real-time.

The traditional Programmable Logic Controller (PLC) in industries cannot support real-time data acquisition from various sensors and the processing of signals. The real-time simulators utilizing multiprocessors [20] such as, General Purpose Processors (GPP) or Digital Signal Processors (DSP) face certain limitations in the field of control, data acquisition, fast processing of digital input/output at the SCADA level and also lack hardware flexibility [21]. The upcoming control algorithms offer faster control using parallel operations, and to take advantage of the potential parallelism the need for parallel computation of system parameters is essential. Therefore, FPGA a reconfigurable I/O hardware interface that is capable to offer high hardware flexibility and computation speed is a promising solution. A comparative study is performed for the real-time simulators that identify the advantages of FPGAs for complex applications [22].

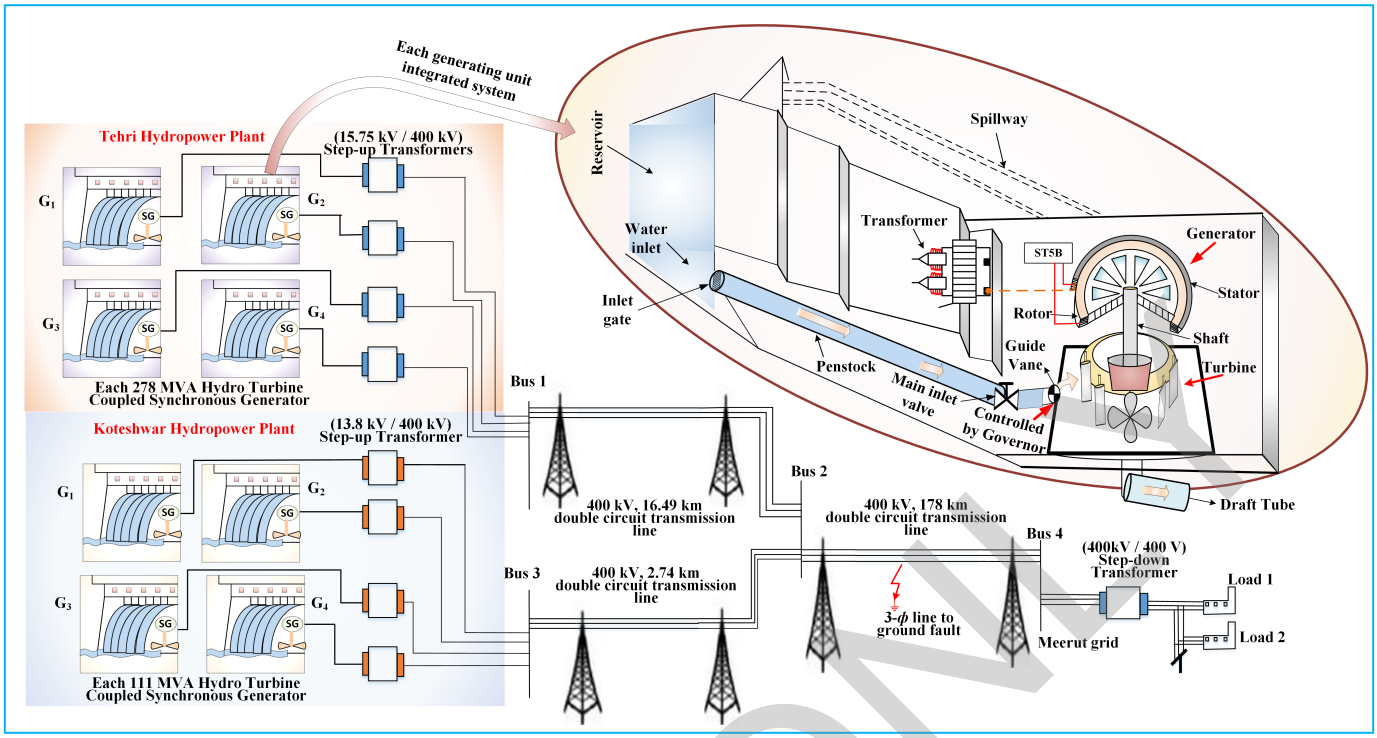

Fig. 1. Overview of Tehri Koteshwar hydropower plant connected to 400kV grid with an extended representation of integrated hydraulic, mechanical and electrical components of each generating unit.

Over the last decade, advancement in both hardware architecture and the software tools of the FPGA boards, prompted them as mainstream processors in many industrial areas. The distributed hardware resource in FPGA are reconfigurable, which can be changed depending on the system model to maximize the computational performance. FPGAs are being used for hardware-in-the-loop (HIL) application for detailed device-level modeling of various power system for power systems [23] and power electronics components [24], [25], [26]. Therefore, in this paper FPGA is used for faster-than-real-time implementation; this FPGA based model produces 49 times faster than real-time implementation making it a unique HPP model implementation and providing a way for online control tuning techniques, system state parameter estimation, data acquisition, and processing during transients for online control, control hardware-in-the-loop testing, and field experiments for HPP in future. The main objective behind FPGA implementation is to overcome the constraint of fast computation requirement of 0.2s-0.3s [11] for online control algorithm implementation in complex systems. This paper emulates a faster-than-real-time HPP model having 8 generators, their controls, and an AC grid network on high-performance Xilinx Virtex® UltraScale + XCVU9P FPGA board. This FPGA board supports high parallelism and pipelined hardware architecture being a 16 nm device with a maximum of 3.8 M system and programmable logic cells, 6840 DSP slices, and 32.75 GB/s maximum transceiver speed.

C. Contribution

The main contributions of the paper are:

- Proposed detailed nonlinear HMEC model of multi-machine HPP bridging gap for various LFO stability studies.
- Improved dynamic stability with robust HTGS PID tuning using Hopf bifurcation and retuning of PSS3B considering HTGS time delay for inter-area oscillation damping.
- Established model accuracy with validation using field measurement data of 1400MW HPP.
- Faster than real-time dynamic hardware emulation of HPP model on FPGA board.
- Testing prototype for parameters effect on stability of HPPs during various electro-mechanical and hydro-mechanical frequency oscillations.

The paper is organized as follows, Section II presents detailed modeling for each component of the power plant. The HTGS solution stability analysis and tuning of the PID controller are presented in Section III followed by model validation using field data in Section IV. Section V presents the transient simulation methodology for system solution using numerical method. Section VI describes the hardware emulation of the model on FPGA and lastly, Section VII presents the conclusion and future perspectives.

II. Mathematical Model of the HPP

The HPP is a complex integrated system of hydraulic, mechanical, and electrical components; Fig. 2 represents the schematic of each generating unit integrated system. To model HPP close to the actual system the nonlinear characteristics of each component are included. For instance, in the HTGS nonlinear characteristics included are servo motor delay, dead-zone, rate limiter, and saturation. In the penstock system,

the water hammer effect is included and for the turbine, the nonlinear model is formed using external characteristics. For the electrical system, ST5B static excitation system, PSS (PSS3B) saturation blocks with lead-lag filters and the 6th order model of synchronous generator is implemented. More detailed description of the mathematical model components and control selection is presented in [27].

A. Governor model

The governor control uses frequency control mode with the power feedback having droop e_p [28]. The deviation in system frequency and the generating unit power with droop e_p add to provide the control for the guide vane opening. The governor control block diagram is shown in Fig. 3. The servo time delay represented by τ affects the phase difference between ω and mechanical power (P_m) which in turn affects the damping of oscillations. Therefore, to reflect the real-time characteristics of the servo system it is important to consider the time delay. The time delay for this system is 0.29s. The vane opening position y, with servo motor delay is given by (1) and (2):

$$\dot{y} = \frac{1}{T_y}((k_p * u + k_i * u_I + k_d * u_d) - y(t-\tau)), t\epsilon\,[\tau, +\infty], \tag{1}$$

$$\dot{y} = \frac{1}{T_y}((k_p * u + k_i * u_I + k_d * u_d) - y_o),\ t\,\epsilon\,[0, \tau]). \tag{2}$$

where $u_I = \int(\Delta P * e_p) * dt + x_4$, $u = \Delta P * e_p + x$, $u_d = (\Delta\dot{P} * e_p + \dot{x})$, $x_4 = \int x * dt$, ΔP is the generator power deviation and $x = (\omega_{ref} - \omega)$ is the generator speed deviation.

B. Penstock model

The penstock and the water column characteristics like water inertia, water compressibility, pipe wall elasticity and water hammer effect during transients have a high impact on the operation of the turbine [29]. Consequently, including the elasticity of penstock and water interia factor the transfer function of the penstock system [30] is expressed as:

$$G_h(s) = \frac{H(s)}{Q(s)} = -h_w\left[\frac{T_r s + \frac{1}{24}T_r^3 s^3}{1 + \frac{1}{8}T_r^2 s^2}\right]. \tag{3}$$

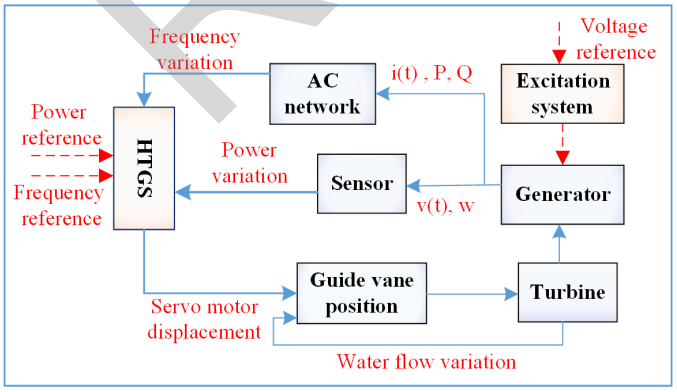

Fig. 2. Functional block schematic of integrated components of the Tehri Koteshwar HPP.

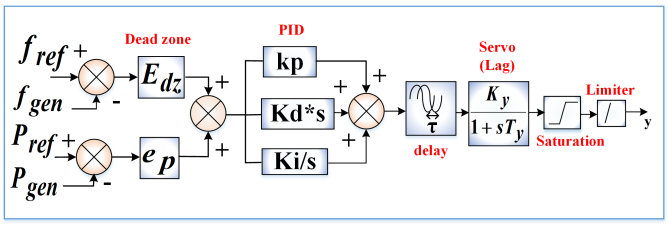

Fig. 3. Block diagram representation of the governor control.

From (3) the differential equations of penstock is obtained as shown in (4)

$$\begin{aligned} \dot{x_1} &= x_2 - \frac{3}{T_w}h \quad ; \quad \dot{x_2} = x_3, \\ \dot{x_3} &= -\frac{24}{T_r^2}x_2 + \frac{48}{T_r^2 T_w}h \quad ; \quad q = x_1, \end{aligned} \tag{4}$$

where, x_1, x_2, x_3 are the state variables, h is the water head, q is the flow rate, h_w, T_r and $T_w = (h_w * T_r)$ are characteristic constant,reflection time and water inertia time constant of the penstock respectively. The HPP model has 4 units each having separate waterways.

C. Turbine model

The HPP model has a variable head vertical Francis turbine with rated head of $188m$. The nonlinear model of the hydro turbine is represented using the external characteristics because of its higher accuracy [31]. The variable transfer coefficients e_y, e_x, e_h, e_{qy}, e_{qx}, e_{qh} are used to represent nonlinear characteristics of turbine in form of (6), where the variable x, y, h, q and m_t are the relative deviations in speed, guide vane opening, head, flow, and torque, respectively. The coefficients $e_y = \frac{\partial m_t}{\partial y}$, $e_x = \frac{\partial m_t}{\partial x}$, $e_h = \frac{\partial m_t}{\partial h}$, $e_{qy} = \frac{\partial q}{\partial y}$, $e_{qx} = \frac{\partial q}{\partial x}$, and $e_{qh} = \frac{\partial q}{\partial h}$ are the partial derivatives of the torque and discharge respectively whose value differ with the operating point and calculated using (5):

$$\begin{aligned} e_y &= e_{ym}(h+1) \quad ; \quad e_x = e_{xm}\sqrt{(h+1)}, \\ e_h &= e_{hm} \quad ; \quad e_{qy} = e_{qym}\sqrt{(h+1)}, \\ e_{qx} &= e_{qxm} \quad ; \quad e_{qh} = e_{qhm}\left(\frac{1}{x+1}\right). \end{aligned} \tag{5}$$

where e_{ym}, e_{xm}, e_{hm}, e_{qym}, e_{qxm}, e_{qhm} are the maximum values of the coefficients at no-load conditions. Thus, the turbine equation is given by (6),

$$\begin{aligned} m_t &= e_y y + e_x x + e_h h, \\ q &= e_{qy} y + e_{qx} x + e_{qh} h. \end{aligned} \tag{6}$$

Using (4) and (6) yields:

$$\dot{h} = \frac{1}{e_{qh}}\left[\frac{e_{qx}(e_g - 2e_x)}{T_{ab}}x + \left(\frac{e_{qy}T_{ab} - E_{qx}e_y T_y}{T_y T_{ab}}\right)y - \left(\frac{e_{qx}e_h}{T_{ab}} + \frac{3}{T_w}\right)h + x_2 - \frac{e_{qy}}{T_y}U + \frac{e_{qx}}{T_{ab}}m_{g0}\right]. \tag{7}$$

where, $U = (k_p u + k_i u_I + k_d u_d)$ and T_{ab} is inertia time constant of the generator. Now combining the equations of

all the above models the HTGS is represented as follows:

$$\begin{aligned}
\dot{x_1} &= x_2 - \frac{3}{T_w}h \quad ; \quad \dot{x_2} = x_3, \\
\dot{x_3} &= -\frac{24}{T_r^2}x_2 + \frac{48}{T_r^2 T_w}h \quad ; \quad \dot{x_4} = x, \\
\dot{x} &= \frac{1}{T_{ab}}\left[(e_g - 2e_x)x - e_y y - e_h h + m_{g0}\right], \\
\dot{y} &= \frac{1}{T_y}\left[k_p u + k_i u_I + k_d u_d - y\right], \\
\dot{h} &= \frac{1}{e_{qh}}\left[\left(\frac{e_{qx}(e_g - 2e_x)}{T_{ab}}\right)x + \left(\frac{e_{qy}T_{ab} - E_{qx}e_y T_y}{T_y T_{ab}}\right)y - \right. \\
&\left. \left(\frac{e_{qx}e_h}{T_{ab}} + \frac{3}{T_w}\right)h + x_2 - \frac{e_{qy}}{T_y}U + \frac{e_{qx}}{T_{ab}}m_{g0}\right].
\end{aligned} \tag{8}$$

D. Generator model and excitation system

The dynamics of a synchronous generators having two d-axis windings and two q-axis damper windings in rotor circuit are represented using 6-dimensional differential equation given by (9) [36]:

$$\begin{aligned}
\dot{\delta} &= \omega_r * \Delta\omega(t), \\
\Delta\dot{\omega}(t) &= \frac{1}{2H}(T_m - T_e - D\Delta\omega(t)), \\
\dot{\psi}_{fd}(t) &= \omega_r\{e_{fd}(t) - R_{fd}i_{fd}(t)\}, \\
\dot{\psi}_{1d}(t) &= -\omega_r R_{1d} i_{1d}(t), \\
\dot{\psi}_{1q}(t) &= -\omega_r R_{1q} i_{1q}(t), \\
\dot{\psi}_{2q}(t) &= -\omega_r R_{2q} i_{2q}(t).
\end{aligned} \tag{9}$$

The static excitation system ST5B with a PSS (PSS3B) [13] is shown in Fig. 4. The differential equations derived for the PSS are given by (10) and for excitation system are given by (11).

$$\begin{aligned}
\dot{v_5} &= \frac{1}{T_1}(k_{s1}P - v_5) \quad ; \quad \dot{v_6} = \frac{1}{T_{w1}}(T_{w1}\dot{v_5} - v_6), \\
\dot{v_7} &= \frac{1}{T_2}(k_{s2}\Delta f_T - v_7) \quad ; \quad \dot{v_8} = \frac{1}{T_{w2}}(T_{w2}\dot{v_7} - v_8), \\
\dot{v_9} &= \frac{1}{T_{w3}}\{T_{w3}(\dot{v_6} + \dot{v_8}) - v_9\}, \\
\ddot{v}_{10} &= \frac{1}{A_4}(v_9 + \dot{v_9}A_1 + \ddot{v_9}A_2 - \dot{v}_{10}A_3 - v_{10}) \\
\dot{v}_{11} &= \frac{1}{A_8}(v_{10} + \dot{v}_{10}A_5 + \ddot{v}_{10}A_6 - \dot{v}_{11}A_7 - v_{11}).
\end{aligned} \tag{10}$$

$$\begin{aligned}
\dot{v_1} &= \frac{1}{T_{r1}}(v_T - v_1), \\
\dot{v_2} &= \frac{1}{T_{b2}}((\dot{V}_{ref} - \dot{v}_1 + \dot{v}_{11})T_{c2} + (V_{ref} - v_1 - v_2 + v_{11})), \\
\dot{v_3} &= \frac{1}{T_{b1}}(\dot{v_2}T_{c1} + v_2 - v_3); \quad \dot{v_4} = \frac{1}{Tr2}(K_r v_3 - v_4), \\
\dot{E}_{fd} &= \frac{1}{T_{r3}}(v_4 - k_c i_{fd} - E_{fd}).
\end{aligned} \tag{11}$$

Here, P, Δf, V_T, V_{ref}, E_{fd} and I_{fd} are active power, speed deviation, terminal voltage, reference voltage, excitation voltage and excitation current of the generator respectively.

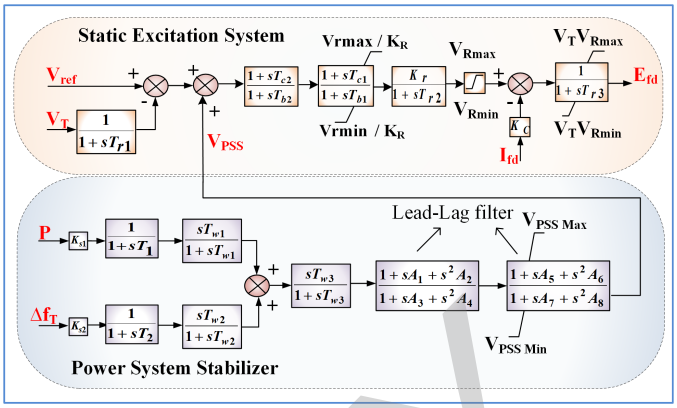

Fig. 4. Static excitation system (ST5B) and power system stabilizer (PSS3B).

The modeled HTGS system is coupled with the electrical system through parameter $\Delta\omega$ as can be seen from $\Delta\dot{\omega}$ expression in (9) that is $x = \Delta\omega$, $m_t = \Delta T_m$ and $m_{g0} = \Delta T_e$ in p.u. During the system solution, the HTGS state parameter value of x and m_t is obtained in each iteration and is used in the solution of the integrated electrical system.

E. AC Network

The 400kV, 178km double circuit, pi-modeled TL network connects two power stations to the load side grid as shown in Fig. 1. The network is represented by a set of algebraic equations, given as:

$$\begin{bmatrix} \mathbf{I_m} \\ \mathbf{I_r} \end{bmatrix} = \begin{bmatrix} \mathbf{Y_{mm}} & \mathbf{Y_{mr}} \\ \mathbf{Y_{rm}} & \mathbf{Y_{rm}} \end{bmatrix} \begin{bmatrix} \mathbf{V_m} \\ \mathbf{V_r} \end{bmatrix}, \tag{12}$$

where m is the number of generator buses and r is the remaining buses. When calculating the current for only generator buses:

$$\mathbf{I_m} = \mathbf{Y_{red}} * \mathbf{V_m}, \tag{13}$$

where $\mathbf{Y_{red}} = \mathbf{Y_{mm}} - (\mathbf{Y_{rm}}.\mathbf{Y_{red}}^{-1}.\mathbf{Y_{mr}})$ and $\mathbf{Y_{red}} = (\mathbf{G} + \mathbf{jB})$, where $\mathbf{G}$ is conductance and $\mathbf{B}$ is inductive susceptance.

III. PID TUNING OF HTGS

For this model the HTGS is a 7 dimension nonlinear system, with time delay due to servo motor. To predict the bifurcation point of the PID controller and identify the stability region of PID parameters Hopf bifurcation technique is used.

A. Hopf bifurcation criteria in model with time delay

The criteria for Hopf bifurcation is given by Theorem 1 with its proof established in [32], [33]:

Theorem 1: For a nonlinear system $\dot{\mathbf{X}} = \mathbf{f}(\mathbf{X}, \mu)$, $\mathbf{X} \epsilon \mathbf{R^7}$, $\mu \epsilon R^1$ where μ is the bifurcation parameters and $\mathbf{f} \epsilon C^\infty$, with an equilibrium point $\mathbf{X} = \mathbf{0}$, the characteristic equation of Jacobian matrix on this equilibrium point is

$$p(\lambda, \mu) = det(\lambda \mathbf{I_7} - \mathbf{A}(\mu)), \tag{14}$$

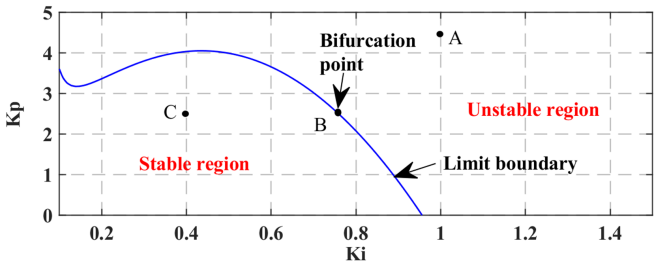

Fig. 5. Bifurcation curve of HTGS with $k_d = 4$.

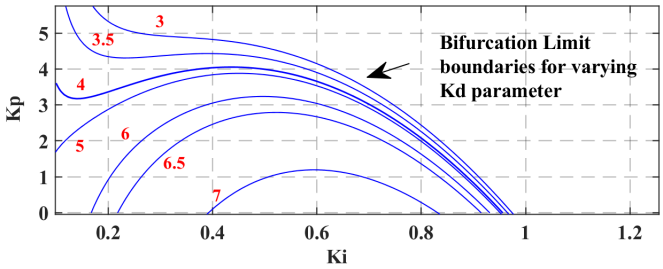

Fig. 6. Bifurcation curve of HTGS with variable k_d.

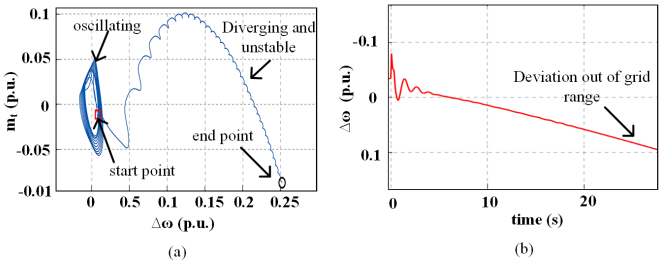

Fig. 7. For PID parameters at Point A in bifurcation graph: (a) phase portrait for Point A; (b) time-domain waveform for Point A.

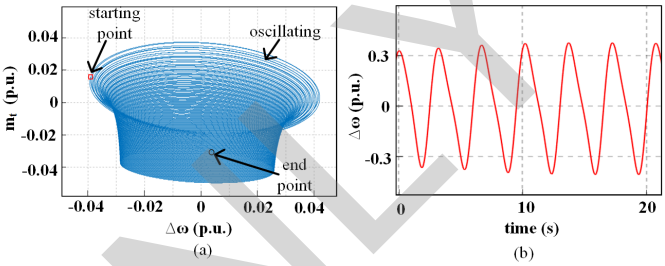

Fig. 8. For PID parameters at Point B in bifurcation graph: (a)phase portrait for Point B; (b) time-domain waveform for Point B.

where $\mathbf{A}$ is the Jacobian matrix when the system has no time delay. With the delayed mathematical model, the characteristic equation is given by

$$p(\lambda, \mu) = det(\lambda \mathbf{I_7} - \mathbf{A}(\mu) - \mathbf{B}(\mu)e^{-\lambda\tau}), \qquad (15)$$

where $\mathbf{A}$ is the matrix with respect to variables having no delay and B is the matrix with respect to delayed variables. To obtain a polynomial characteristic equation, $e^{-\lambda\tau}$ is replaced using pade approximation $e^{-\lambda\tau} = \frac{(1-\lambda\tau)}{(1+\lambda\tau)}$, thereafter rearranging,

$$p(\lambda, \mu) = p_n(\mu) * \lambda^n + p_{n-1}(\mu) * \lambda^{n-1} + \ldots + p_0 \quad .(16)$$

The calculation of polynomial characteristic equation of the system is presented in Appendix A. The Hopf bifurcation occurs when $p(\lambda, \mu)$ has a pair of imaginary roots $\pm i\omega$ at $\mu = \mu_0$ (bifurcation point), that is alternatively established if the following conditions are satisfied:

1. All coefficients $p_i > 0$, where $i = 1, 2, 3, \ldots, n$ so that there are no positive roots.

2. If $p_i = 0$, where $0 < i < n$ then $Det(\mathbf{L_n}) > 0$, and the sub determinants of $\mathbf{L_n}$ are all greater than zero except $Det(\mathbf{L_{n-1}}) = 0$.

Here, $\mathbf{L_n} = \begin{pmatrix} p_1(\mu) & p_0(\mu) & \cdots & 0 \\ p_3(\mu) & p_2(\mu) & \cdots & 0 \\ \vdots & \vdots & \ddots & \vdots \\ p_{2n-1}(\mu) & p_{2n-2}(\mu) & \cdots & p_n(\mu) \end{pmatrix}$.

- $\mathbf{L_1} = p_1(\mu), \quad Det(\mathbf{L_1}) > 0,$
- $\mathbf{L_2} = \begin{pmatrix} p_1(\mu) & p_0(\mu) \\ p_3(\mu) & p_2(\mu) \end{pmatrix}, \quad Det(\mathbf{L_2}) > 0,$
- Similarly for all $\mathbf{L_i}$, $0 < i \leq n$, except $\mathbf{L_{n-1}}$, where $Det(\mathbf{L_{n-1}}) = 0$.

Now, the above stated conditions are used to identify the bifurcation curve and the stability region of each PID parameter. Using the first condition of Theorem 1 $p_i > 0$, the range of the k_d is obtained by putting $p_2 > 0$. The coefficient $p_2 = 10.39 - 1.63k_d$, therefore the $k_d < 6.374$. Using the second condition $Det(\mathbf{L_{n-1}}) = 0$ and choosing a value of $k_d = 4$ within its stability range an implicit 2 variable polynomial representing relation between k_p and k_i is obtained. The polynomial is given by $f(k_p, k_i) = 3.956 * 10^3 k_p - 4.075 * 10^3 k_i - 6.0463 * 10^4 k_p k_i + 8.94 * 10^5 k_i^2 - 9.297 * 10^5 k_i^3 + 0.59$. The plot of polynomial called bifurcation limit boundary is shown in Fig. 5. Any point on the bifurcation line will result in imaginary roots of the characteristic equation leading to oscillations in the system. Consider a point B as shown in Fig. 5 as the bifurcation point where k_i is considered as the bifurcation parameter μ; the values of $k_p = 2.5$, and k_i is 0.77. The system is tested with bifurcation point B set as PID parameters and it lead to oscillations as can be seen in Fig. 7, due to imaginary roots of the characteristic equation at this point. Therefore, PID parameters value lying on the curve shown in Fig. 5 are critical points, the values below the curve are stable, and the ones above are unstable. To ensure stable operation of the system and better transient response, PID parameters must be selected from the stable region and preferable away from the curve or the limit boundary. To further analyse the stability region boundary of k_p and k_i using bifurcation curve, these curves are plotted for varying values of k_d as shown in Fig. 6. From Fig. 6 it is observed that with the increasing value of k_d the stability region of k_p and k_p parameters decreases and when k_d value goes above 6.5 the stability region of k_p is quite low to provide sufficient gain to the frequency error in the governor control to maintain stability.

This article has been accepted for publication in IEEE Transactions on Industry Applications. This is the author's version which has not been fully edited and content may change prior to final publication. Citation information: DOI 10.1109/TIA.2024.3439254

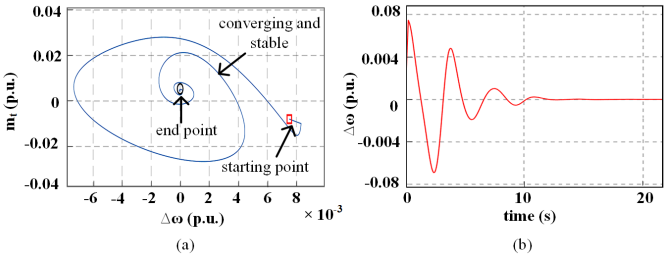

Fig. 9. For PID parameters at Point C in bifurcation graph: (a) phase portrait for Point C; (b) time-domain waveform for Point C.

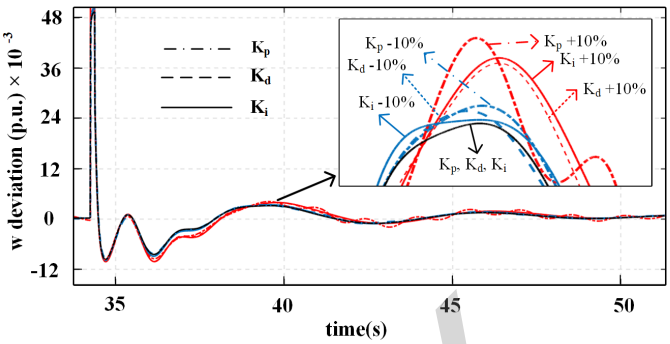

Fig. 10. PID parameter sensitivity for $\Delta\omega$ dynamic response.

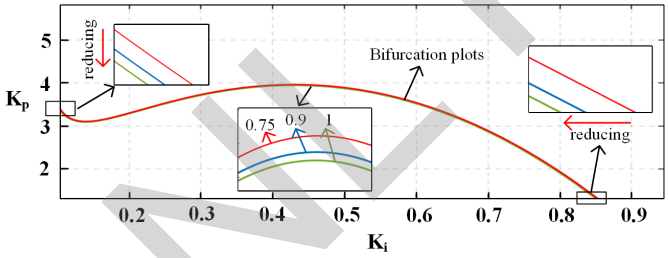

Fig. 11. Stable domain of PID parameters with power variation.

Therefore, for wider and reliable stability region $k_d = 4$ is chosen and three sets of k_p and k_i values are considered denoted by points A, B, and C in Fig. 5. For each set of values, the system stability is analysed using phase portrait and time-domain waveform of the system parameters. The phase portraits show the deviation in turbine torque against the generator speed. In the phase portrait figures, the red marker is the starting point and the black marker is the ending point. The time-domain waveforms show the response of the generator speed deviation. For Point A $k_p = 4.5$ and $k_i = 1$, the phase portrait as shown in Fig. 7(a) diverges, and the time waveform of the speed deviation in Fig. 7(b) increases and deviation range goes out of grid recommended deviation, leading to system instability. For the Point B, $k_p = 2.5$ and $k_i = 0.75$, the phase portrait as shown in Fig. 8(a) oscillates around the equilibrium point but fails to converge. The time-domain waveform of speed deviation in Fig. 8(b) shows that oscillations last for a long duration eventually leading to system instability. For the Point C, $k_p = 2.5$ and $k_i = 0.4$, the phase portrait as shown in Fig. 9(a) converges to the equilibrium point and the time-domain waveform in Fig. 9(b) shows that the speed deviation is 0, therefore the stability is achieved. Thus, Point C lies in the stability range of the PID parameter and will be used in the system for further study. The range of PID parameters is quite defined from the above process but trial-and-error tuning method is required to obtain optimal operating point within this range.

B. Sensitivity study

To ensure the stability of the tuned model, PID Parameter sensitivity analysis using system state variable and the sensitivity study of load variation on the PID parameter stability region is performed. For PID Parameter sensitivity each PID parameter k_p, k_i and k_d is varied 10% while keeping the other two parameters constant. The parameter sensitivity is studied here using the rotor speed deviation $\Delta\omega$ of the generator. From Fig. 10 it can be seen that even with 10% parameters variation, the system is stable after a 3-phase fault at 34s. Also, the rotor speed deviation has higher sensitivity to k_p as can be seen in Fig. 10, as $k_p + 10\%$, and the $k_p - 10\%$ has the highest peaks as compared to others. To study sensitivity for load variation, modeled system stability for tuned parameters during 3 loading condition is performed. The Hopf bifurcation curves for 1, 0.9 and 0.75 p.u. power loading are shown. As seen in the extended parts of the Hopf bifurcation plot in Fig. 11, the intersection point of the stable region with the x- axis and y-axis is reducing with the increase in power rating. This means that the variation range of k_p and k_i is reduced with increase in power that can otherwise be also said as, for same value of PID parameters but with higher power rating the pressure to ensure stability is higher. Therefore, it is suggested to choose values of k_p and k_i in stable regions far from the bifurcation line so as to maintain better stability during sudden large variation which is also followed here for selecting the PID parameters.

IV. Model Validation

The HPP model accuracy is validated using the field data from the HPP. The NRLDC report [12] stated that this 3-phase fault led to undamped oscillation of 0.6Hz near Bus 1 (as shown in Fig. 1) and eventually Unit-I of plant was tripped. The field data of Unit I at Tehri station is recorded during a 3-phase fault using Supervisory Control and Data Acquisition (SCADA) and is presented in Fig. 12. The generator loading, governor and excitation system parameters used in the model for the comparison are same as those of the real power plant used during the fault. This recorded field data is compared with the modeled system in Fig. 13. When considering the fault at 34s, the Fig. 13(a) shows the vane position, Fig. 13(b) shows the rotor speed, Fig. 13(c) shows the generator terminal voltage, and Fig. 13(d) shows the rotor field current. The vane position and the speed are directly related to governor control; the generator terminal voltage and the rotor field current are directly related to excitation control. As seen from the Fig. 13 the fault led to undamped oscillations initially for 16s and 21s after the fault finally lead to the sudden shutdown of the generator (Unit I). Moreover, after 50s as

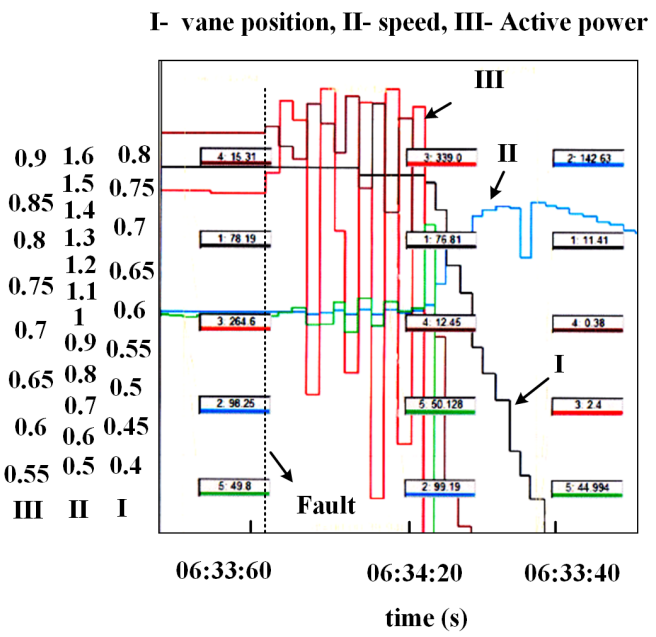

Fig. 12. SCADA measurement for 250MW generator tripping during sustained inter-area oscillation.

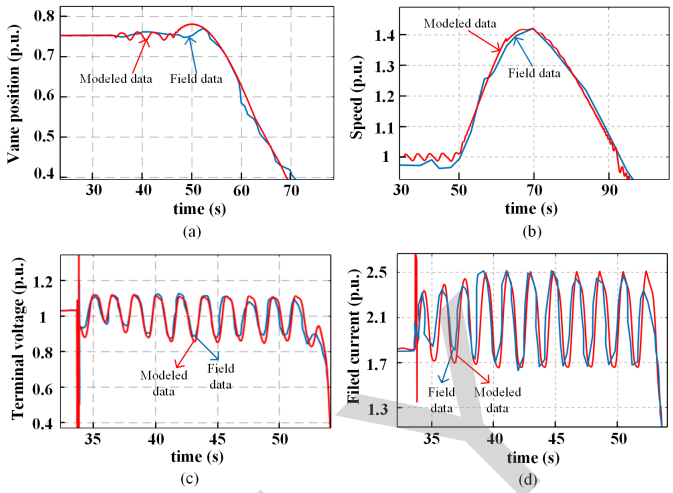

Fig. 13. Model comparison with field data: (a) guide vane position; (b) rotor speed; (c) generator terminal voltage; (d) rotor field current.

seen in Fig. 13(a) the vane closes very rapidly, and in Fig. 13(b) rotor speed increases from 1 p.u. to 1.42 p.u and finally reduces to zero. Fig. 13(c) shows that the generator terminal voltage has undamped oscillations of around 0.6Hz for 16s after the fault and then within another 4s voltage in Fig. 13(c) and field current in Fig. 13(d) drops leading to tripping of the generating unit at 54s. The response from the plant and the model show a good resemblance. However, some of the differences seen in the comparative results are due to model parameters approximation, like characteristic curves of the turbine, imprecise waterway system measurement and variation in sub-transient or transient time constant of the generator model. Also differences due to measurement sampling and filtering sensors are inevitable. This model is used for real-time application in FPGA, with new tuned control system parameters of governor and excitation system which presents improved transient stability.

V. Transient Simulation Procedure

To simulate the complete model both algebraic equations from the AC network and differential equations from each HPP component combination need to be solved. The overall system is represented in form of a first-order differential algebraic equation (DAE), where $\mathbf{X_n}$ is a vector of state variables and $\mathbf{V}$ is a vector of bus voltages, $\mathbf{I}$ is a vector of injected currents in the buses and $\mathbf{Y}$ is admittance matrix with initial conditions $(\mathbf{X_{n0}}, \mathbf{V_0}, \mathbf{I_0})$ obtained using load flow:

$$\dot{\mathbf{X}}_\mathbf{n} = \mathbf{f}(\mathbf{X_n}, \mathbf{V}), \tag{17}$$

$$\mathbf{I}(\mathbf{X_n}, \mathbf{V}) = \mathbf{Y_N V}. \tag{18}$$

For the solution of a set of higher-dimensional nonlinear differential equations, a time-domain numerical method is required. For a complex set of equations, certain numerical methods can be unstable unless an extremely small time step is used, which increases computation complexity. However, the explicit Runge-Kutta 4th order (RK4) method is a widely used numerical method known for its high stability and accuracy [34], [35] and is employed here. The system is solved with the partitioned approach, using the explicit RK4 method for differential equations and the Gauss-Seidel method for nonlinear algebraic equations. This technique offers good programming flexibility and robustness [36]. During transients, such as grid fault at time t, the state variables of the system do not change instantaneously. Firstly, using the present state vector $\mathbf{X_n}$, solution of algebraic equations (18) gives $\mathbf{V}$ and $\mathbf{I}$ at time t. Then, the state vector $\mathbf{X_n}$ and the voltage vector $\mathbf{V}$ are used to calculate $\dot{\mathbf{X}}_\mathbf{n}$ vector using the RK4 method and lastly the $\mathbf{X_n}$ vector is calculated using $\dot{\mathbf{X}}_\mathbf{n}$ at $t = t + \Delta t$ where Δt is the time-step.

VI. Hardware Emulation on FPGA

The Xilinx Virtex® UltraScale+™ XCVU9P FPGA board containing 1182240 look-up tables (LUTs), 2364480 flip-flops (FFs), and 6840 DSP slices is used for emulation of HPP. The FPGA integrated circuit enables parallel and pipelined hardware structure emulation of the HPP system which accelerates the control, prediction, and stability of the system. To emulate the hardware, firstly the HPP model is programmed in Xilinx Vitis® software. The Fig. 14. shows a flow chart for the methodology of FPGA emulation. The software Vitis® is a high-level synthesis package that allows writing the algorithm of hardware modules in C++ called as C simulation and converts it into hardware languages like Verilog and VHDL. Using this software, hardware description language (HDL) code is optimized to achieve minimum latency and resource utilization in FPGA. The C++ code is optimized using various pragmas to have a proper interface and pipelining of the functions or modules called as code optimization. The coding technique and pipeline pragmas work as the foundation for parallel execution and flow acceleration. Each component of

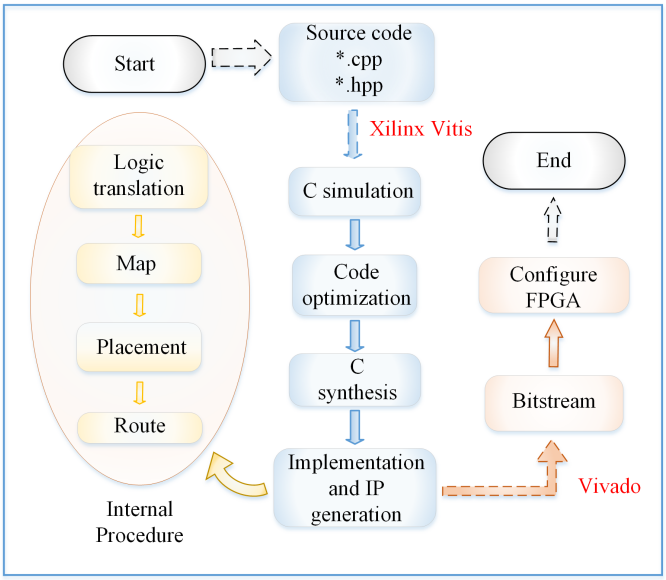

Fig. 14. Flowchart of model implementation on FPGA.

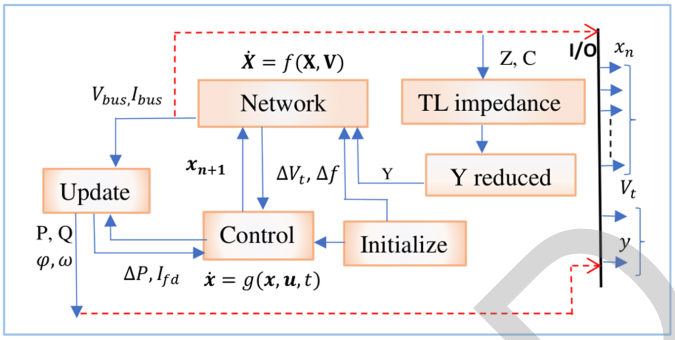

Fig. 15. Hardware design modules and signal flow route in FPGA emulation.

TABLE II
HARDWARE MODULES RESOURCE UTILIZATION IN FPGA

Module	DSP	FF	LUT	Latency
Initialize	792	110021	318110	188T_{clk}
Control	865	113290	81405	237 T_{clk}
Y_{TL}	0	33	2029	32T_{clk}
$Y_{reduced}$	691	154224	104497	818T_{clk}
Network	123	18021	17458	494T_{clk}
Update	171	39816	24453	288T_{clk}
Resource used	1727	306957	384858	2050T_{clk}
Percentage	(25.2%)	(12.98%)	(32.55%)	-
XCVU9P	6840	2364480	1182240	-

the HPP system is coded as a C++ function; each function is called module in harware design and its signal flow route is shown in Fig. 15. Hardware design has 6 modules named *TL impedance*, $Y_{reduced}$, *initialize*, *control*, *network*, and *update*. The *initialize* function performs the system parameters initialization. The *control* module has HTGS and excitation system differential equations; its iterative solution using the RK4 numerical method obtains the state variable of the control system such as guide value opening, torque from the turbine, speed of the turbine, rotor slip, excitation voltage and PSS output. The $Y_{reduced}$ module uses *TL impedance* module having

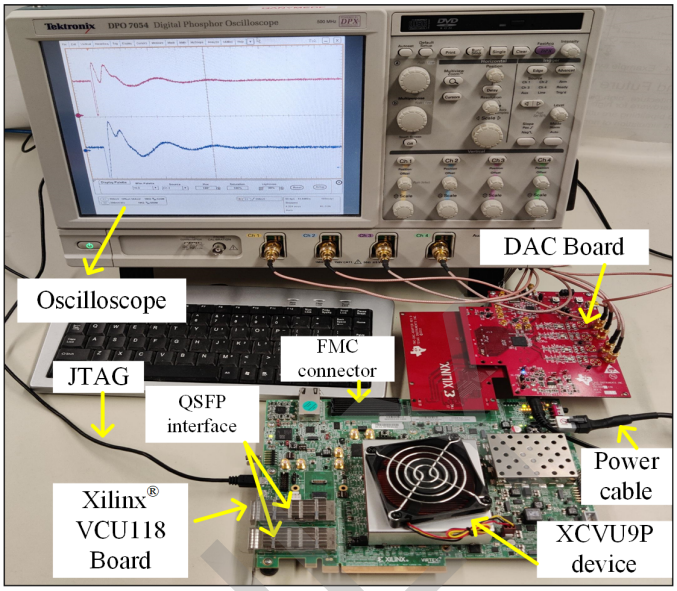

Fig. 16. FPGA hardware setup for real-time emulation of the HPP.

TL parameters to calculate the Y bus matrix required for the power flow equations. The *network* module then uses the admittance from $Y_{reduced}$, state variables from the *control* module, and generator parameters to solve the power flow equations of the system. Using the obtained system parameters the power from each generator, excitation current, and fluxes of the machines are updated in the *update* module to be used for the next iteration. The solution of the system is identified using the iterative loop execution of these modules or functions.

The time-step for dynamic simulation required is 1ms for solution convergence; however, using the advantage of parallel computation of FPGA, each function is solved in parallel by unrolling the loops for the functions which accelerates the computation of the system's dynamic solution. After optimization of the code using pragmas in Xilinx Vitis®, the code is fully parallelized for minimum latency and resource utilization. As shown in Table I the resource utilization is about 33 % and the total latency of the functions is 2050 T_{clk}, where the T_{clk} is the clock cycle of the FPGA taken as 10ns. Thus, the total time required for each iteration in FPGA is 2050 × 10ns = 20.5 μs. Therefore, due to parallel computation, the FPGA hardware emulation is $\frac{1ms}{20.5\mu s} \approx$ 49 times faster than the dynamic simulation.

The code is then synthesized into RTL IP design. The synthesized code is verified using co-simulation before exporting it to Vivado® which creates bitstream using the RTL IP. The bitstream is downloaded from the host computer in the FPGA board via JTAG interface. The output data from the board is converted from digital to analog using a digital and analog converter (DAC) in the FPGA Mezzanine Card (FMC). The results then can be displayed on the oscilloscope as shown in Fig. 16.

This implementation of the HPP on FPGA can be used in a real power system, where the data from the real system is sent to the control center that is taken as input to FPGA. There are three bidirectional ports for high-speed data input-output,

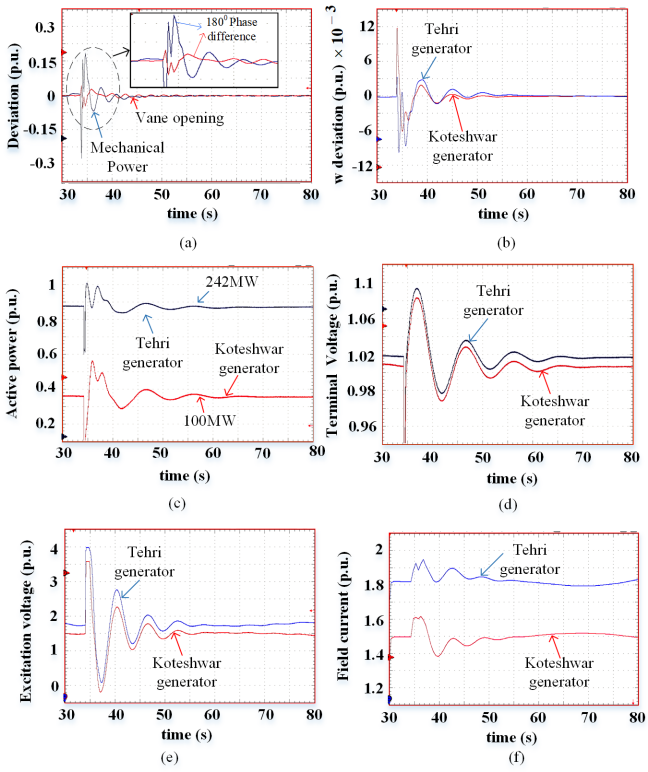

Fig. 17. Real-time simulation results displayed on the oscilloscope: (a) mechanical power and governor vane deviation of Tehri generator; (b) rotor speed deviation of Tehri and Koteshwar generator; (c) active power of Tehri and Koteshwar generator; (d) voltage at bus 1 and bus 3; (e) rotor excitation voltage of Tehri and Koteshwar generator; (f) rotor excitation current of Tehri and Koteshwar generator.

via Samtec® FireFly connector, Quad Small Form-factor Pluggable (QSFP) interface, and Ethernet interface. Using this data system analysis, control, prediction, or decision-making during contingencies can be performed. Due to the high speed of computation, it provides enough time for decision-making or online control technique implementation.

A. FPGA emulation results and validation

To analyze the transient stability of the system a 3-phase fault at 34s for 100ms on the TL between bus 2 and 4 as shown in Fig. 1 is considered. The same fault scenario as discussed in section IV is considered. As presented in the Fig.13 due to fault 0.6Hz sustained oscillation lead to tripping of the generating unit-I. The governor's PID parameters obtained from the hopf bifurcation stability criteria are used here. Fig. 17 shows the oscilloscope results, where 1 division in the oscilloscope presents 100 ms which refers to 1 s on the x-axis. As the FPGA emulation is 49 times faster than real-time execution, the oscilloscope can represent the signal waveform for approximately 50s. Fig. 17(a) shows the deviation in mechanical power and governor vane opening; due to water inertia, the phase difference between them is approximately 180° which is a typical characteristic response of a non-minimum system. The governor vane opening limiter limits the deviation to 0.1 p.u./s, as can also be seen clearly in Fig. 17(a) and this denotes the slow response of the mechanical system

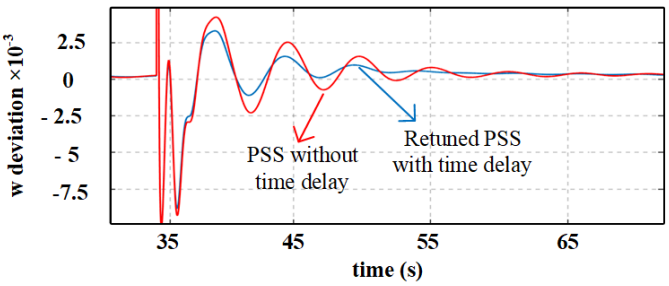

Fig. 18. Dynamic response of $\Delta\omega$ with different PSS gain.

which in return affects the speed of tracking changes in the power. The deviations due to the fault in power and governor vane opening converge to 0 in 28s after the fault, regaining the system stability. The transient oscillations damping performance depends on the phase difference between the speed and the power which is greatly influenced by the governor time delay being 0.29s for this system. This damping performance is improved by increasing the PSS gain k_{s1} and k_{s2} from 2.4 and -0.5 to 4.8 and -0.8 respectively. The difference is damping performance with PSS without considering the time delay in HTGS and with PSS considering the time delay is shown in Fig. 18. With enhanced damping the speed stability is achieved 10s faster and a reduction of 33.2% in overshoot of rotor speed $\Delta\omega$ deviation is seen. The Fig. 17(b) is the rotor speed deviation of one of the generators at Tehri and Koteshwar stations each; stability is assured as the speed deviation is within the permissible limits of the grid code. Here, having the system base as 278MVA Fig. 17(c) shows the active power from 250MW generator at Tehri operating at a rating of 0.87 p.u. and 100MW generator at Koteshwar operating at a rating of 0.36 p.u. Fig. 17(d) is bus voltage profile of the Tehri bus and Koteshwar bus, where the bus at Tehri is at 1.02 p.u. the and bus at Koteshwar is 1.01 p.u. Fig. 17(e) and Fig. 17(f) show the excitation voltage and excitation currents of the generators respectively. The oscillation in terminal volatge and excitation voltage are damped in 18s compared to that in Fig. 13 showed sustained oscillations for 21s and then leading to instability. For the tuned parameters of HTGS, and PSS (PSS3B) the HPP has attained stability for transient and can damp out oscillations efficiently. The effect of nonlinear servo motor delay is also compensated.

VII. Conclusion

The proposed nonlinear HMEC model of HPP and hopf bifurcation stability analysis overcomes the constraint of linearizing the system focused for a particular type of low frequency oscillation study. Proposed model accuracy is validated through a test case using field-data from the grid. In the case study transient stability analysis is performed for 3-phase fault that led to sustained 0.6Hz inter area oscillations and tripping of 250MW generator. For better stability robust tuning of governor's PID is attained while considering nonlinear HTGS and penstock model. The negative damping effect of HTGS servo-motor delay is identified and 10 secs faster stability is attained by improved tuning of PSS. Also, 49 times faster

than real-time HPP model is emulated on FPGA board. This emulation of complete HPP model prospects as a generic testing lab prototype that can be used for stability analysis during various low-frequency oscillations and their resonance effect on HPPs stability connected to grid. In future this study can be extended for the following:

- New control strategies and its hardware-in-the-loop testing.
- Integration stability study of HPP connected with cascaded pumped storage variable speed hydro power plants and other renewable resources with easy extendibility in FPGA and optimal hardware resource utilization and lesser latency.
- System security assessment.
- Fault analysis and plant optimization.
- Faster than real-time state estimation for prediction of cascading failures using real-time data, or during unavailability of PMU data due to sensor fault or cyber-attacks.

APPENDIX

A. Hopf bifurcation polynomial equation

The polynomial characteristic equation for Hopf bifurcation is $p(\lambda,\mu) = det(\lambda I_7 - A(\mu))$, where A and B are

$$\text{A} = \begin{pmatrix} 0 & 1 & 0 & 0 & 0 & 0 & -1.071 \\ 0 & 0 & 1 & 0 & 0 & 0 & 0 \\ 0 & -8.304 & 0 & 0 & 0 & 0 & 5.932 \\ 0 & 0 & 0 & 0 & 1 & 0 & 0 \\ 0 & 0 & 0 & 0 & -0.08 & 0 & -0.166 \\ 50 & 0 & 0 & 71.43*ki & {A_{65}}^* & 0 & 11.9*kd \\ 0 & 1 & 0 & -20*ki & {A_{75}}^* & 0 & {A_{77}}^* \end{pmatrix}$$

$${A_{75}}^* = 0.0193 - 0.13*k_p + 1.61*k_d$$

$${A_{65}}^* = 71.43*k_p - 5.75*k_d$$

$${A_{77}}^* = 1.388 + 0.016*k_d$$

$$\text{B=} \begin{pmatrix} 0 & 0 & 0 & 0 & 0 & 0 & 0 \\ 0 & 0 & 0 & 0 & 0 & 0 & 0 \\ 0 & 0 & 0 & 0 & 0 & 0 & 0 \\ 0 & 0 & 0 & 0 & 0 & 0 & 0 \\ 0 & 0 & 0 & 0 & 0 & -0.111 & 0 \\ 0 & 0 & 0 & 0 & 0 & 7.93*k_d - 71.43 & 0 \\ 0 & 0 & 0 & 0 & 0 & 1.402 + 2.22*k_d & 0 \end{pmatrix}$$

Using the matrices A and B
$p(\lambda,\mu) = det(\lambda I_7 - A(\mu) - B(\mu)e^{-\lambda\tau})$,

$p(\lambda,\mu) = 0.1x^8 + (10.39 - 1.63k_d)x^7 + (126.87 - 15.075k_d - 0.793k_p)x^6 + (-302.4 - 6.19k_p + 148.8k_d + 0.458k_i + 0.212{k_d}^2 - 0.0041k_dk_p)x^5 + (1599 - 93.94k_d + 27.76k_i + 134.2k_p - 2.71{k_d}^2 + 0.041k_dk_p - 2.62k_dk_ix^4 + (-2.04*10^3 + 1251.2k_d - 53.577k_p - 252.84k_i + 26.3k_dk_i - 0.34k_dk_p + 1.76{k_d}^2)x^3 + (174.6 + 262.6k_d + 354k_i + 1.12*10^3*k_p + 0.34k_d*k_p - 21.8k_dk_i - 17.58{k_d}^2x^2) + (153.9 + 2.12k_p - 2*10^3k_i - 24.4k_d + 218.4k_dk_i)x + 328.75k_i.$

B. System parameters

Tables III, IV, V, VI give parameters of the system components.

TABLE III
GOVERNOR, PENSTOCK, TURBINE

$E_{dz} = \pm 0.005$	$k_y = 5$	$Vg_{min} = -0.1$	$e_{qhm} = 0.75$
$k_p = 2.5$	$T_y = 0.07$	$T_w = 2.8$	$e_{qym} = 1.05$
$k_d = 4$	$g_{max} = 1.0$	$T_{ab} = 10.8$	$e_{ym} = 1.2$
$k_i = 0.4$	$g_{min} = 0.01$	$T_r = 1.7$	$e_{xm} = -0.85$
$e_p = 0.05$	$Vg_{max} = 0.1$	$e_{qxm} = -0.18$	$e_{hm} = 1.8$

TABLE IV
ST5B EXCITATION SYSTEM PARAMETERS

$T_1 = 0.02$	$T_{B2} = 0.01$	$T_{OB2} = 0.08$	$K_R = 210$
$T_{C1} = 0.8$	$T_{OC1} = 0.1$	$V_{Rmax} = 3.8$	$T_2 = 0.04$
$T_{B1} = 6$	$T_{OB1} = 0.2$	$V_{Rmin} = -3.6$	-
$T_{C2} = 0.08$	$T_{OC2} = 0.08$	$T_1 = 0.02$	-

TABLE V
PSS3B DUAL INPUT POWER SYSTEM STABILIZER PARAMETERS

$A_1 = 0.359$	$A_7 = 0.031$	$T_{w2} = 1.5$
$A_2 = 0.586$	$A_8 = 0$	$T_{w1} = 1.5$
$A_3 = 0.429$	$T_1 = 0.02$	$K_{s1} = 4.5$
$A_4 = 0.564$	$T_2 = 0.02$	$K_{s2} = -0.8$
$A_5 = 0.001$	$V_{PSSMin} = -0.075$	$T_{w3} = 0.6$
$A_6 = 0$	$V_{PSSMax} = 0.075$	-

TABLE VI
SYNCHRONOUS GENERATOR

Parameters	**250MW generator**	**100MW generator**
Stator Voltage L-L (kV)	15.75± 5%	13.8± 5%
Frequency	50± 3%	50± 3%
Rotor V (Volts), $I_f(A)$	300, 1600	240, 1125
$R_s, R_r(p.u.)$	0.003, 0.000135	0.003, 0.000163
$X_{ad}, X_{1d}, (p.u.)$	1, 0.25	0.978, 0.22
$X_{aq}, X_{1q}(p.u.)$	0.63, 0.3	0.6, 0.28
H, F	5.4, 0.019	4.6, 0.019

REFERENCES

[1] T. Hennig, W. Wang, Y. Feng, X. Ou, and D. He, "Review of Yunnan's hydropower development. Comparing small and large hydropower projects regarding their environmental implications and socio-economic consequences," *Renew. and Sust. Energy Reviews*, vol. 27, pp. 585-595, 2013.

[2] Z. Peng, X. Chen and L. Yao, "Research status and future of hydro-related sustainable complementary multi-energy power generation," *Sust. Futures*, vol. 3, art.no. 100042, 2021.

[3] D. N. Konidaris and J. A. Tegopoulos, "Investigation of oscillatory problems of hydraulic generating units equipped with Francis turbines," *IEEE Trans. on Energy Conv.,* vol. 12, no. 4, pp. 419-425, Dec. 1997.

[4] S. P. Mansoor, D. I. Jones, D. A. Bradley, F. C. Aris and G. R. Jones, "Reproducing oscillatory behaviour of a hydroelectric power station by computer simulation," *Control Engineering Practice,* vol. 8, no. 11, pp. 1261–1272, 2000.

[5] J. C. Mantzaris, A. Metsiou and C. D. Vournas, "Analysis of Interarea Oscillations Including Governor Effects and Stabilizer Design in South-Eastern Europe," *IEEE Trans. on Power Syst.,* vol. 28, no. 4, pp. 4948-4956, Nov. 2013.

[6] H. N. Villegas Pico, D. C. Aliprantis, J. D. McCalley, N. Elia and N. J. Castrillon, "Analysis of Hydro-Coupled Power Plants and Design of Robust Control to Damp Oscillatory Modes," *IEEE Trans. on Power Syst.,* vol. 30, no. 2, pp. 632-643, March 2015.

[7] X. Liu and C. Liu, "Eigenanalysis of Oscillatory Instability of a Hydropower Plant Including Water Conduit Dynamics," *IEEE Tran. on Power Syst.,* vol. 22, no. 2, pp. 675-681, May 2007.

[8] P. C. O. Silva, C. Nicolet, P. Grillot, J. -L. Drommi and B. Kawkabani, "Assessment of Power Swings in Hydropower Plants Through High-Order

Modeling and Eigenanalysis," *IEEE Trans. on Ind. Appl.,* vol. 53, no. 4, pp. 3345-3354, Aug. 2017.
[9] W. Yang, P. Norrlund, J. Bladh, J. Yang and U. Lundin, "Hydraulic damping mechanism of low-frequency oscillations in power systems: a quantitative analysis using a nonlinear model of hydropower plants," *Applied Energy,* vol. 212, pp. 1138-1152, Feb. 2018.
[10] H. Zhang, D. Chen, B. Xu and F. Wang, "Nonlinear modeling and dynamic analysis of hydro-turbine governing system in the process of load rejection transient," *Energy Conv. and Manag.,* vol. 90, pp. 128-137, Jan. 2015.
[11] B. Xu, J. Zhang, M. Egusquiza, D. Chen, F. Li, P. Behrens and E. Egusquiza, "A review of dynamic models and stability analysis for a hydro-turbine governing system," *Renew. and Sust. Energy Reviews*, vol. 144, art.no. 110880, 2021.
[12] "Northern Regional Power Committee (Transmission Planning) Report," Central Elect. Authority (India), Tech. Rep. CEA-PS-11-21(19)/3/2019-PSPA-I, 2020. Accessed: Jun. 15, 2021 [Online]. Available: https://cea.nic.in/wp-content/uploads/pow_sys_pan_com/2021/02/MoM_2nd_NRPCTP.pdf 2018.
[13] *"IEEE Recommended Practice for Excitation System Models for Power System Stability Studies,"* IEEE Std. 421.5, 2016.
[14] R. Tiwari and T. R. Chelliah, "Design improvement and tuning of excitation system ST5B with PSS3B and coordinated OEL in hydropower plant," *IEEE Trans. on Ind. Appl.,* vol. 58, no. 5, pp. 5895-5907, Sept. 2022.
[15] V. Ajjarapu and B. Lee, "Bifurcation theory and its application to nonlinear dynamical phenomena in an electrical power system," *IEEE Trans. on Power Syst.,* vol. 7, no. 1, pp. 424-431, Feb. 1992.
[16] S. H. Strogatz, *Nonlinear Dynamics and Chaos: with Applications to Physics, Biology, Chemistry, and Engineering*, Boca Raton: CRC Press, 2015.
[17] D. Ling and Y. Tao, "An analysis of the Hopf bifurcation in a hydro turbine governing system with saturation," *IEEE Trans. on Energy Conv.*, vol. 21, no. 2, pp. 512-515, June 2006.
[18] J. Li and Q. Chen, "Nonlinear dynamical analysis of hydraulic turbine governing systems with nonelastic water hammer effect," *Journal of applied math.,* vol. 2014, no. (SI23), pp. 1-11, 2014.
[19] F. Wang, D. Chen, B. Xu and H. Zhang, "Nonlinear dynamics of a novel fractional-order Francis hydro-turbine governing system with time delay", *Chaos, Solitons & Fractals,* vol. 91, pp. 329-338, Oct. 2016.
[20] M. L. Scala, G. Sblendorio, A. Bose, and J. Q.Wu, "Comparison of algorithms for transient stability simulations on shared and distributed memory multiprocessors," *IEEE Trans. Power Syst.,* vol. 11, no. 4, pp. 2045–2050, Nov. 1996.
[21] F. Streit, S. Wituschek, M. Pschyklenk, A. Becher, M. Lechner, S. Wildermann, I. Pitz, M. Merklein and J. Teich, "Data acquisition and control at the edge: a hardware/software-reconfigurable approach," *Prod. Eng. Res. Devel.*, vol. 14 pp. 365–371, 2020.
[22] A. Malinowski and H. Yu, "Comparison of embedded system design for industrial applications," *IEEE Trans. on Ind. Info.*, vol. 7, no. 2, pp. 244-254, May 2011.
[23] S. Jin, Z. Huang, R. Diao, D. Wu and Y. Chen, "Comparative implementation of high-performance computing for power system dynamic simulations," *IEEE Trans. on Smart Grid,* vol. 8, no. 3, pp. 1387-1395, May 2017.
[24] S. Cao, N. Lin and V. Dinavahi, "Faster-than-real-time dynamic simulation of AC/DC grids on reconfigurable hardware," *IEEE Trans. on Power Syst.,* vol. 35, no. 2, pp. 1539-1548, March 2020.
[25] S. Cao, N. Lin and V. Dinavahi, "Damping of sub-synchronous control interactions in large-scale PV installations through faster-than-real-time dynamic emulation," *IEEE Access,* vol. 9, pp. 128481-128493, 2021.
[26] V. Dinavahi and N. Lin, *Real-Time Electromagnetic Transient Simulation of AC-DC Networks*, Wiley IEEE press, 2021.
[27] R. Tiwari, T. R. Chelliah and V. Dinavahi "Non-linear Hydromechanical and Electrical Coupled Model of 1400MW Hydropower Plant for Governor Tuning Application," *Proc. IEEE Inter. Conf. on Energy Tech. for Future Grid,* Dec. 2023.
[28] W. Yang, P. Norrlund, C. Yung Chung, J. Yang, U. Lundin, "Eigenanalysis of hydraulic-mechanical-electrical coupling mechanism for small signal stability of hydropower plant," *Renew. Energy,* vol. 115, pp. 1014-1025, 2018.
[29] B. Xu, D. chen, H. Zhang, F. Wang, "Modeling and stability analysis of a fractional-order Francis hydro-turbine governing system," *Chaos, Solitons Fractals,* vol. 75, pp. 50-61, 2015.
[30] G. A. Munoz-Hernandez,S. P. Mansoor, D.I. Jones, *Modelling and Controlling Hydropower Plants*, Netherlands: Springer London, 2012.
[31] H. Li, D. Chen, H. Zhang, F. Wang, D. Ba, "Nonlinear modeling and dynamic analysis of a hydro-turbine governing system in the process of sudden load increase transient," *Mechanical Syst. and Signal Proc.,* vol. 80, pp. 414-428, 2016.
[32] B. D. Hassard and N. D. Kazarinoff, *Theory and Applications of Hopf Bifurcation*, Cambridge, UK: Cambridge Univ. Press, 1981.
[33] W.M. Liu, "Criterion of Hopf Bifurcations without Using Eigenvalues," *Journal of Mathematical Analysis and Appl.*, vol. 182, no.1, pp. 250-256, 1994.
[34] A. Bellen and M. Zennaro, *Numerical Methods for Delay Differential Equations*, UK: Oxford university press, 2003.
[35] H. Chengming, F. Hongyuan and L. Shoufu, "Stability analysis of Runge-Kutta method for non-linear delay differential equations," *BIT Numerical Mathematics,* vol. 39, pp. 270–280, 1999.
[36] P. Kundur, *Power System Stability and Control*, New York: McGraw-Hill, 1994.

Ritu Tiwari (Student member, IEEE) received her B.Tech. degree in electrical engineering from Nirma University, Institute of Technology, India, in 2018, and M.Tech. degree in Water Resource Development and Management (WRDM), Indian Institute of Technology Roorkee (IITR), India, in 2020. She is currently pursuing a joint Ph.D. in power systems with IITR, Roorkee, India, and the University of Alberta, Canada. Her research interests include hydropower system transient analysis and control, power transient state estimation, real-time simulation, and field-programmable gate arrays.

Thanga Raj Chelliah (Senior Member, IEEE) received the Diploma degree from the Government Polytechnic College, Nagercoil, India, in 1996, the B.Eng. degree from the Coimbatore Institute of Technology, Coimbatore, India, in 2002, the M.Eng. degree from the Government College of Engineering, Tirunelveli, India, in 2005, and the Ph.D. degree from IIT Roorkee, Roorkee, India, in 2009, all in electrical engineering. He is currently an Associate Professor with the Department of Water Resources Development and Management, IIT Roorkee, where he is also a Faculty-in-Charge with the Hydropower Simulation, Power Electronics, and Hydro-Electric Machines Laboratories. His research interests include power electronics applications in large-rated pumped storage plants, asynchronous generators, and marine propulsion systems. Dr. Chelliah is also a Senior Member of the IEEE Industry Applications Society and the IEEE Industrial Electronics Society, a member of the IEEE Standards Association, a Life Member of the Indian Water Resources Society, and an Alternate Member of the Hydroelectric Powerhouse Structures Sectional Committee, Bureau of Indian Standards. He is also an Associate Editor of the IEEE Transactions on Energy Conversion and Transportation Electrification Community eNewsletter.

Venkata Dinavahi (Fellow, IEEE) received the B.Eng. degree in electrical engineering from Visvesvaraya National Institute of Technology (VNIT), Nagpur, India, in 1993, the M.Tech. degree in electrical engineering from the Indian Institute of Technology (IIT) Kanpur, India, in 1996, and the Ph.D. degree in electrical and computer engineering from the University of Toronto, Ontario, Canada, in 2000. He is currently a Professor with the Department of Electrical and Computer Engineering, University of Alberta, Edmonton, Alberta, Canada. He is a Fellow of the Engineering Institute of Canada. His research interests include real-time simulation of power systems and power electronic systems, electromagnetic transients, device level modeling, large-scale systems, and parallel and distributed computing.